MIT Libraries | DSpace@MIT

MIT Open Access Articles

Discovering Amorphous Indium Phosphide Nanostructures with High-Temperature ab Initio Molecular Dynamics

Massachusetts Institute of Technology

Discovering Amorphous Indium Phosphide Nanostructures with High-Temperature *Ab Initio* Molecular Dynamics

Qing Zhao[1,2], Lisi Xie[1], and Heather J. Kulik[1,*]

[1]*Department of Chemical Engineering, Massachusetts Institute of Technology, Cambridge, MA 02139*
[2]*Department of Mechanical Engineering, Massachusetts Institute of Technology, Cambridge, MA 02139*

ABSTRACT: We employ high-temperature *ab initio* molecular dynamics (AIMD) as a sampling approach to discover low-energy, semiconducting, indium phosphide nanostructures. Starting from under-coordinated models of InP (e.g. a single layer of InP(111)), rapid rearrangement into a stabilized, higher-coordinate but amorphous cluster is observed across the size range considered (In_3P_3 to $In_{22}P_{22}$). These clusters exhibit exponential decrease in energy per atom with system size as effective coordination increases, which we define through distance-cutoff coordination number assignment and partial charge analysis. The sampling approach is robust to initial configuration choice as consistent results are obtained when alternative crystal models or computationally efficient generation of structures from sequential addition and removal of atoms are employed. This consistency is observed across the 66 structures compared here, and even when as many as five approaches are compared, the average difference in energy per pair of atoms in these structures is only 1.5 kcal/mol at a given system size. Interestingly, the energies of these amorphous clusters are lower than geometry optimized spherical models of bulk InP typically used for simulations of quantum dots. Favorable energetics appear correlated to highly-coordinated indium and phosphorus with coordination numbers up to five and seven, respectively, as well as formation of phosphorus-phosphorus bonds.

1. Introduction

Nanostructured materials exhibit unique properties with respect to their bulk counterparts, and first-principles simulation can provide valuable insight into their unusual structure-property relationships. Semiconducting quantum dots (QDs) in particular have drawn the attention of a broad scientific community because they exhibit unique size- and shape-dependent electronic and optical properties[1]. QDs have demonstrated their technological relevance in a broad number of applications including in fluorescence labeling for biotechnology[2-3], light-emitting diodes[4-5], solar cells[6-7], and lasers[8-9]. Although CdSe QDs were the first to be developed with controllable size[10] in large quantity with emission across the visible range[11], alternative QDs have been sought due to the high toxicity[12] of cadmium. InP QDs have since been identified as one of the most promising alternatives to CdSe both because of their broader emission color range and lack of intrinsic toxicity[13-15]. Nevertheless, preparation of high-quality InP QDs has remained challenging, despite ongoing efforts to understand and direct the nucleation and growth mechanisms during synthesis[14-18].

Several groups have carried out semi-empirical, tight-binding[19] and DFT[20-24] studies of InP nanowires[20-22] and the related core-shell InAs/InP nanowires[23-24] as well as studies of bulk InP surfaces[25-27] both pristine and in the presence of water. InP QDs are comparatively less well studied with only a few semi-empirical, tight-binding[28-29] or hybrid DFT[30] studies. In some of these cases, the surface has been passivated with neutral[20] or partially charged[21, 30] hydrogen atoms, oxygen atoms[20], or methyl groups[29], while in other cases an unpassivated surface[20, 28] is studied. Regardless of passivation approach, typically the experimental bulk crystal structure geometry is used[22] and at most a local geometry optimization[30] is carried out on the experimental starting structure. Studies of bulk crystal models and geometry optimized models have also been

carried out on QDs comprised of CdSe[31-33], PbSe[32-33], and PbS[34] both with[31, 34] and without[32-34] ligand passivation. A key challenge for studying InP nanostructures is that InP QDs have been characterized with a crystalline core but relatively disordered, partially oxidized amorphous shell that appears to limit further growth of InP QDs[14]. Part of the amorphous shell is attributed to the breakdown and reaction of the carboxylate ligands used in precursors to synthesize InP QDs, and the full extent of the structure of the surface of these QDs is not known. No attempts have been made to model or sample potential amorphous structures of InP QD surfaces. Related transition-metal phosphide materials (e.g., with iron, nickel, or zinc) are known to be amorphous[35], and computational approaches suitable for study of InP could also be useful for transition-metal phosphide materials.

Despite the lack of study of amorphous InP surfaces, a great deal of computational effort has been dedicated to obtaining low energy configurations of other types of nanostructures. One of the most popular approaches is the coalescence kick method, in which atoms are randomly placed far apart and then pushed towards the center of mass until they coalesce into a cluster that is roughly the size of the pairwise sums of known covalent radii. This search is repeated many times, and the most stable structure after optimization with DFT is hypothesized to be the global minimum[36]. This approach has been fruitfully applied to small clusters such as Pt_8[37], Mg_{17}[38], AlB_3H_{2n} (n=0-6)[39], and Ge_{10}[40]. High computational demands and large numbers of possible random structures have limited the kick method to small, mostly single element clusters of less than 20 atoms. Low energy structures of similarly sized metallic (e.g. Au_{20}[41]) and bimetallic[42] clusters have been obtained using genetic algorithms combined with DFT to evaluate energies and carry out geometry optimizations[41-43].

3

Minimum hopping methods, in which minima are sought and then propagated away from dynamically with a history list used to avoid revisiting the same minima, that are carried out primarily with tight-binding, have been carried out on small clusters (e.g. 19 atoms of silicon)[44]. Similarly sized clusters, e.g. Si16, have been accessible with metadynamics[45]. In a related approach known as Basin-hopping Monte Carlo, configurations are geometry optimized after the Monte Carlo move, have permitted study of larger 55 atom clusters of Ag and Ag/Pd mixtures when combined with a simplified Lennard-Jones force field[46] or around 33 atom Pt-alloy clusters when a mixture of tight-binding, semi-empirical approaches and DFT are used[47]. Simulated annealing molecular dynamics, in which systems are heated and then slowly-cooled, combined with semi-empirical or classical molecular dynamics has permitted study of larger 50 atom gold clusters[48] or up to 160 atoms of stoichiometric ZnS[49].

In light of the uncertainty regarding the shell structure around InP QDs, we were interested in identifying whether we could discover possible low-energy structures of indium phosphide clusters that have order distinct from the bulk crystal structure. Our goal is to identify candidate surface and cluster structures that are likely to be accessible depending on synthesis conditions, not necessarily identify the global energy minimum for our structures. By not mandating a global minimum search, we may study larger clusters and identify whether alternative structures can be competitive with crystalline order. Our initial inspiration for this approach comes from a recent study[50] in which graphene spontaneously reorganized to form fullerenes during molecular dynamics simulations. Here, we instead employ high-temperature *ab initio* molecular dynamics on models of crystalline InP, e.g. of the InP(111) surface that contains hexagonal bonding structure similar to graphene, and we will demonstrate that this approach encourages reorganization to low energy structures.

The outline of the paper is as follows. In Sec. 2, we present the computational details of our study. Section 3 contains results and discussion on *ab initio* molecular dynamics sampling of clusters, various approaches for generating clusters, and evaluation of electronic and geometric properties of the clusters. We provide conclusions in Section 4.

2. Computational Details

All *ab initio* molecular dynamics (AIMD) simulations and geometry optimizations[51] were carried out with TeraChem[52-53]. AIMD simulations were performed with the Hartree-Fock (HF) method and the 3-21G basis set[54]. Geometry optimizations were carried out using density functional theory (DFT) with the hybrid B3LYP[55-57] exchange-correlation functional and the composite LACVP* basis set. The LACVP* basis set corresponds to an LANL2DZ effective core potential basis for the indium atom and 6-31G* basis for the phosphorus atom. The default B3LYP definition in TeraChem uses the VWN1-RPA form[58] for the local density approximation component of the correlation. In the AIMD simulations, we employ a 0.5 fs timestep and keep a constant temperature of 1000 K with a Langevin thermostat. Resulting trajectories range from 20,000 to 50,000 time steps (10 to 25 ps) in length. For a prototypical system studied here, HF calculations are roughly three times faster than DFT, and minimal basis sets provide similar speed up over the polarized double-zeta basis set. HF calculations are also more robust for convergence to self-consistency, reducing the number of cycles required for a single point energy calculation.

Initial configurations for the AIMD simulations were obtained from models of the experimental zinc blende InP crystal structure. Experimental parameters for the InP structure[59] were obtained from the Crystallography Open Database (COD)[60], which provides a Crystallographic Information File (CIF) that contains the InP unit cell geometry, space group,

and lattice parameter. The super cell builder function in Avogadro[61] was then used to build models of crystallographic planes (InP(111), InP(011), InP(001)) and spherical cuts of the bulk (In_7P_7, $In_{12}P_{12}$, $In_{13}P_{13}$, $In_{22}P_{22}$) by removing unneeded atoms from super cells (see Figure 1). These initial structures ranged in size from 6 atoms to 32 atoms.

InP(111)

InP(011)

$In_{12}P_{12}$

$In_{14}P_{14}$

spherical

InP(001)

$In_{13}P_{13}$

$In_{16}P_{16}$
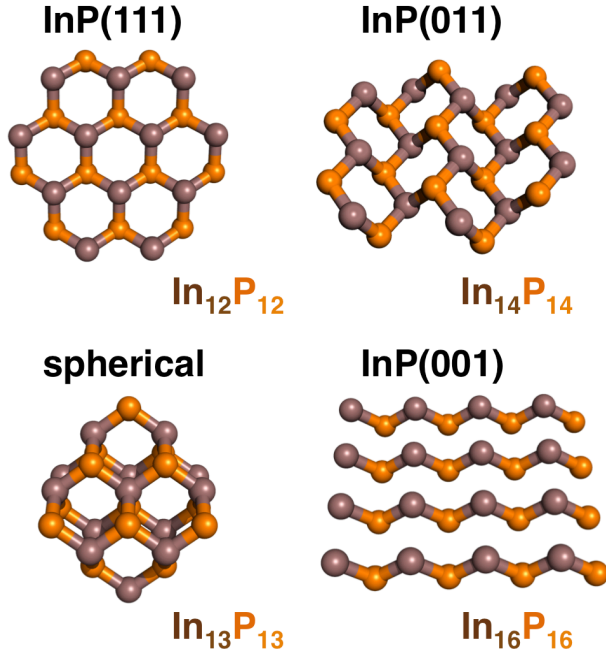
Figure 1. Representative ball and stick models of zinc blende InP clusters, which are starting configurations for high temperature *ab initio* molecular dynamics: single layer models of the InP(111) ($In_{12}P_{12}$, top left), InP(011) ($In_{14}P_{14}$, top right), InP(001) ($In_{16}P_{16}$, bottom right) surfaces as well as a spherical cut of bulk ($In_{13}P_{13}$, bottom left). Indium atoms are brown and phosphorus atoms are indicated in orange.

Coordination numbers of individual atoms are assigned based on rescaled covalent radii of indium and phosphorus, which are 1.42 Å and 1.07 Å[62], respectively. The cutoff for an In-P bond was assigned as:

$$d_{cut}(\text{A-B}) = 1.25 * (r_{cov}(\text{A}) + r_{cov}(\text{B})) \; , \tag{0}$$

6

which is 3.1 Å when A=In and B=P for the In-P bond. For comparison, the nearest-neighbor In-P distance in the experimental zinc blende InP structure is 2.54 Å[59, 63]. Since our cutoff distance for coordination is somewhat arbitrary, we also analyzed the sensitivity of coordination number trends to variations in the distance cutoff of about 10% (that is, ±0.3 Å). When coordination numbers of In by P or vice versa are reported in the results, these analyses are based on d_{cut}(In-P) = 3.1 Å, with results obtained at d_{cut}(In-P) = 2.8 Å and = 3.4 Å in parentheses. Similarly, coordination of phosphorus by another phosphorus atom is identified by P-P distances within d_{cut}(P-P) = 2.7 Å. Voronoi polyhedron analysis with the Voro++ code[64] is used to characterize amorphous structures.

Partial charges of atoms were obtained from the TeraChem interface with the Natural Bond Orbital (NBO) v6.0 package[65]. NBO calculates the natural atomic orbitals (NAOs) for each atom by computing the orthogonal eigenorbitals of the atomic blocks in the density matrix, and the NBO partial charge on an atom is obtained as the difference between the atomic number and the total population for the NAO on the atom.

3. Results and Discussion

3a. AIMD sampling for cluster generation

We have performed high-temperature (1000 K) *ab initio* molecular dynamics (AIMD) on a 24 atom model of a single layer of the InP(111) surface. The model InP(111) structure has a slightly non-planar, hexagonal shape due to tetrahedral bond angles around In and P (Figure 1). We note that our simulation temperature is lower than the experimental melting point (1343 K) for crystalline InP[66], but it is above the typical temperature for InP quantum dot synthesis (450 K)[14, 16-18]. Since our simulation only includes indium and phosphorus atoms, rearrangements of the InP(111) model in the AIMD trajectory are completely defined by average instantaneous In-

P, In-In, and P-P distances (Figure 2). During the very initial stages of the high temperature MD run (Figure 2), all average distances briefly increase before they plateau and then decrease substantially. While InP(111) surface atoms are tetrahedral with three-fold coordination in-plane of In and P, the isolated sheet first becomes planar, increasing average distances. Following this initial increase, the layer then buckles, with edge atoms folding inward to form a second layer of InP where the fold has occurred. More local folding events occur until the structure becomes globular.
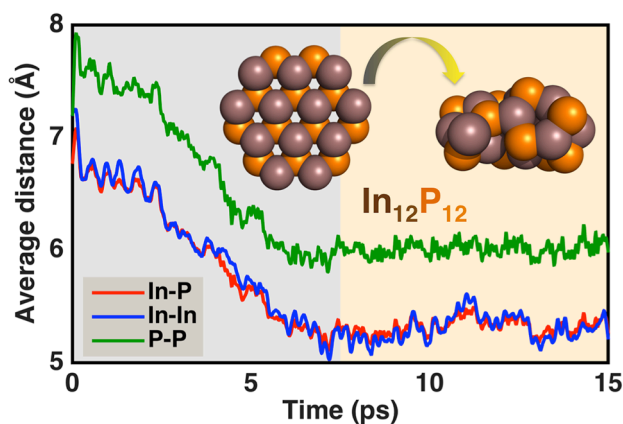
Figure 2. Average distances of In-P (red line), In-In (blue line), and P-P (green line) for the $In_{12}P_{12}$ cluster over time from *ab initio* molecular dynamics. The average distances for all bond types have a region of monotonic decline (gray shaded region) followed by a leveling off with small oscillations (orange region). A representative initial and final structure of $In_{12}P_{12}$ is indicated in inset (indium atoms are brown van der Waals spheres and phosphorus atoms are orange van der Waals spheres).

The formation of the three-dimensional cluster leads to rapid, approximately linearly, decreasing average distances over the first 7.5 ps of the AIMD trajectory. A linear best fit to obtain the rate of change of average distances between In and P atoms is obtained as:

8

$$d_{avg}(\text{In-P}) = -0.25t + 6.90 \ ,\tag{0}$$

where $d_{avg}(\text{In-P})$ is the average distance in Å and the simulation time, t, is in ps. Similarly, the time evolution of the average In-In distances may be obtained with the same -0.25 Å/ps slope but with a larger intercept of 6.97 Å. These two relationships may be compared to the time evolution of the average distance of all phosphorus atoms:

$$d_{avg}(\text{P-P}) = -0.29t + 7.83 \ ,\tag{0}$$

where $d_{avg}(\text{P-P})$ is in Å and t is in ps. The larger P-P intercept is due to larger initial increases in P-P distances, which is then compensated by a slightly steeper slope (-0.29 Å/ps). Once the coalescence period has completed, all average distances stabilized for the remainder of the simulation (an additional 7.5 ps), with constant averages $d_{avg}(\text{In-In})$=5.3 Å, $d_{avg}(\text{In-P})$=5.3 Å, and $d_{avg}(\text{P-P})$=6.0 Å. The total energy of the cluster is correlated to the structural rearrangement into a globular cluster, with a rapid reduction in energy during the coalescence period followed by a leveling off of the energy at around 7.5 ps (see Supporting Information Figure S1). Instantaneous fluctuations ($\sim$ 0.1 Å) in average distances between time steps are nearly the same in the coalescence and in the stabilized regimes. Phosphorus atoms on the surface show the single largest variations in position during the simulation, while In atoms both in the core and on the surface exhibit smaller variations.

We then verified that unchanging average distances corresponded to fluctuations about a single energy minimum with geometry optimizations of five isolated snapshots 1.5 ps apart from the 7.5 ps stabilized regime. Geometry optimizations are carried out with B3LYP/LACVP*, and they lead to a reduction in total energy of 77-105 kcal/mol for each snapshot, partially due to corrections in differences between HF/3-21G (used for AIMD) and B3LYP/LACVP* preferred geometries. The final energies of the five geometry optimizations vary by no more than 0.2

kcal/mol, confirming the stabilized regime corresponds to fluctuations around a single minimum energy basin. Semiconducting materials are ideally suited for this computational procedure, but we note HF cannot treat metallic behavior and DFT would need to be used along side fractional occupancy of levels around the Fermi energy and sufficiently delocalized basis functions.

The initial layer of InP(111) was roughly a circle with a 12.7 Å diameter, while the new globular cluster is ellipsoidal with dimensions of 11.9 Å, 7.9 Å, and 5.9 Å. The change in size corresponds to a reduction in surface area of 193 $Å^2$, as determined by van der Waals radii, and a ~250 kcal/mol reduction in energy after geometry optimization. We repeated the high-temperature AIMD at 1200 K, 700 K, and 500 K (see Supporting Information Table S1) in order to identify whether simulation temperature had a significant effect on energetics. Final energies of the all clusters were within 1-2 kcal/mol of the 1000 K structure, but coalescence time increased from 7.5 ps at 1000 K to 15 ps at 700 K and 20 ps at 500 K. The 1200 K cluster coalesced slightly faster at around 6 ps but generated a structure on the higher energy range, suggesting 1000 K is a good compromise between computational efficiency and generation of low energy structures.

The average coordination number (CN) in the optimized cluster is 2.8 (d_{cut} = 2.8 Å: 2.7; d_{cut} = 3.4 Å: 2.8) for In and 3.0 (2.8; 3.0) for P, which is an increase from CN=2.5 for the initial single-layer InP(111) structure. The maximum CN is 3 (3; 3) for In and 4 (3; 4) for P, and 10-11 of the 12 In and P atoms have CN 3 or higher. The minimum CN is 2 (0; 2) for In and 2 (2; 2) for P atoms, and only 1-2 In or P atoms have this low coordination (see Supporting Information Table S2). While the presence of undercoordinated atoms is surprising when associated with a large reduction in surface area, overall higher average CN outweighs the energy penalty of the

few undercoordinated species observed.

Comparison of NBO charges for the optimized clusters (see Supporting Information Table S3) reveals average In and P charges (q) of +1.14 and -1.14, which are larger than +1.01 and -1.01 for the initial InP(111) model. Under-coordinated atoms are more neutral with charges of +0.71 and +1.06 (CN=2) for In atoms and -0.99 (CN=2), -0.76/-0.71 (CN=3) for P atoms. Since In-P bonds are fairly ionic, the degree of In-P charge separation appears to correlate roughly to the strength of bonding. For the initial InP(111) structure, CN=2 boundary indium atoms had a charge of 0.93, while boundary phosphorus atom charges were -0.87. These results suggest that in some cases the CN=2 coordinated atoms in the cluster are in a higher effective coordination environment than the edge atoms in the initial InP(111) cluster. The two outlying CN=3 phosphorus atoms (q= -0.76, -0.71) are in a unique configuration in which one of the three coordinating atoms for each atom is the other phosphorus atom. Phosphorus-phosphorus bonds are covalent, explaining the lower net charge on these P atoms. The two phosphorus atoms form a dimer with a P-P distance of 2.3 Å, which is elongated with respect to the 1.9 Å[67] bond in a gas phase phosphorus dimer due to bonding of the P atoms with other cluster atoms.

3b. Generalizing the sampling approach for different sized clusters

It is interesting to identify whether these AIMD-driven rearrangements are strongly size-dependent by repeating the procedure for 6-28 atom single-layer models of InP(111). The initial configurations range from highly symmetric to more elongated (see Supporting Information Figure S2), where elongated structures (e.g., In_5P_5, In_7P_7, $In_{11}P_{11}$, and $In_{13}P_{13}$) are 4.9 Å wide (7.6 Å for $In_{13}P_{13}$) and 1.7x, 2.5x, or 4.2x longer (2.5x for $In_{13}P_{13}$). The smallest models have nearly 4 times as many two-coordinated atoms as three-coordinated (CN_{avg}=2 in In_3P_3 and In_4P_4), but this ratio decreases to 1.2 in the largest asymmetric model ($In_{12}P_{12}$, $In_{13}P_{13}$, $In_{14}P_{14}$ all have CN_{avg}=2.5)

(see Supporting Information Table S4). The In_3P_3, In_8P_8, In_9P_9, and $In_{10}P_{10}$, models are relatively symmetric with comparable widths and lengths, and the $In_{14}P_{14}$ model is of intermediate symmetry between $In_{12}P_{12}$ and $In_{13}P_{13}$. While all other structures are generated from repeating hexagonal patterns, to satisfy the stoichiometry of In_4P_4 and In_6P_6, single atoms were added to In_4P_4 and a bridge was introduced between two hexagons in In_6P_6.

For nearly all InP(111) structures considered, the high-temperature AIMD simulations exhibit the same rapid, monotonic decrease in average distances corresponding to formation of a globular cluster followed by a leveling off and stabilization of average distances as in $In_{12}P_{12}$ (see Figure 2). The In_3P_3, In_5P_5, In_8P_8, and In_9P_9 clusters required the shortest times (2.5 ps) to reach the stable regime, though the two smaller clusters (In_3P_3 and In_5P_5) did not strictly rearrange to form a globular structure. For the smallest cluster (In_3P_3), large fluctuations in average distances were observed without any rapid decline. Instead, the evenly distributed In-P-In and P-In-P angles in the cyclic structure rearranged to acute In-P-In angles and very obtuse P-In-P angles. The rearrangement for In_5P_5 was similar with an additional breaking of the central link in the originally bicyclic compound and formation of acute In-P-In and obtuse P-In-P angles (see Supporting Information Figure S3). The most asymmetric $In_{11}P_{11}$ layer required the longest time (15 ps) to reach the stable region (see Supporting Information Table S5). Counter to expectations, low-CN atoms on the In_4P_4 model did not accelerate the dynamics, but the singly coordinated atoms in In_4P_4 initiated a second layer in the structure, more closely mimicking nanoparticle-like clusters than In_3P_3 and In_5P_5. Fluctuations of average distances in the stable regime (~0.05-0.1 Å) did not show dependence on the cluster size except for larger fluctuations (up to 0.16 Å) in the three smallest clusters (see Supporting Information Table S6).

The commonality of behavior in AIMD simulations over a wide range of system sizes

12

motivates future work in automating this approach for generating cluster structures from other elements, stoichiometry, and size ranges. The signatures of coalescence and stabilization during the AIMD trajectory provide a path for an automatic method. Coalescence will be identified as follows: after the first 3,000 steps, a running average is computed over 1,000 steps, and a finite difference slope is compared every 500 steps. When the finite difference slope is reduced, zero, or positive twice, the simulation is identified as being in the stabilized regime. The simulation is then continued until the slope remains near zero for 1 ps. We have implemented this automatic method and are currently employing it in ongoing study of other materials.

The energetic properties of the resulting 6-28 atom clusters we generate exhibit a strong size-dependence (Figure 3). In order to examine how the energy depends on cluster size, we define a relative energy per pair of In, P atoms referenced against the energy of the smallest cluster size studied (In_3P_3):

$$E_{\text{per pair}}(n) = \frac{E(In_nP_n)}{n} - \frac{E(In_3P_3)}{3} \quad , \tag{0}$$

where $E(In_nP_n)$ is the energy of cluster In_nP_n and n is the number of In, P pairs. In each case, relative energies are obtained from five optimized snapshots obtained 0.5-2.5 ps apart (see Supporting Information Table S7), as for $In_{12}P_{12}$. The relative energy decreases rapidly from In_3P_3 to In_8P_8 and levels off for the larger sized clusters (In_9P_9 to $In_{14}P_{14}$). This energetic dependence is fit with an exponential trend line of the form:

$$E_{\text{per pair}}(n) = 210(2n)^{-1.05} - 30.5 \tag{0}$$

with a residual of 20.3 kcal/mol. The asymptotic relative energy per pair is -30.5 kcal/mol, and clusters $In_{81}P_{81}$ in size or larger are predicted to be within 1 kcal/mol of the asymptote.
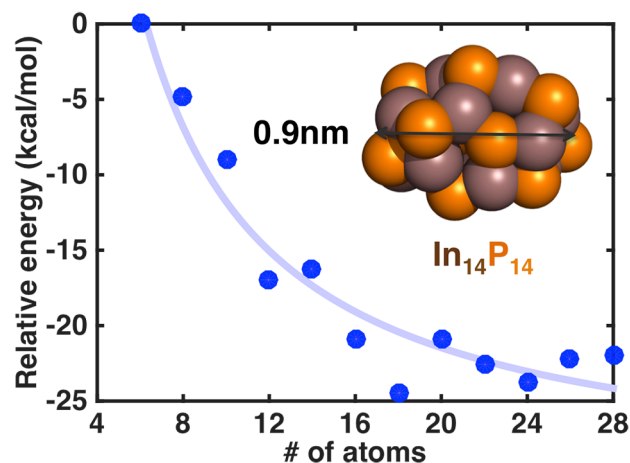
Figure 3. Relative energy per pair of InP atoms (blue dots) as a function of system size referenced against the In_3P_3 cluster. Energies are obtained from averages of geometry optimizations from several snapshots obtained from high temperature *ab initio* molecular dynamics on single layers of the InP(111) surface. The resulting structure of one representative cluster ($In_{14}P_{14}$) is shown in inset along with its corresponding size (indium atoms shown as brown van der Waals spheres and phosphorus atoms are orange van der Waals spheres). An exponential best fit line (light blue) is also shown.

Overall, the diameters of the structures are reduced by 24-37% from the initial InP(111) structures (see Supporting Information Table S8-9) with the diameter reduction increasing with increasing cluster size (see Supporting Information Figure S4), corresponding to an increase in CN as well. The $In_{14}P_{14}$ cluster is about 0.9 nm in diameter, which is in reasonable agreement with previous experimental studies[18] of a cluster with around 14 InP units that was determined to be about 1.1 nm. Average In CN for the clusters range from 2.0 (2.0; 2.0) for In_3P_3 and In_5P_5 to 3.5 (3.0; 3.5) for $In_{10}P_{10}$ and 3.3 (3.2; 3.5) for $In_{13}P_{13}$ with CN increasing as cluster size increases especially from In_3P_3 to $In_{10}P_{10}$ (see Supporting Information Figure S5). As CN averages level off, so do the energies of the clusters. The average P coordination numbers range from 2.0 (2.0; 2.0) for the small clusters (In_3P_3 and In_5P_5) to 3.5 (3.4; 3.6) for larger structures ($In_{10}P_{10}$, $In_{11}P_{11}$,

14

and $In_{13}P_{13}$).

Of the subset of high-CN atoms, we identify buried atoms as CN=4 or higher that are at least one covalent radius (r_{cov}) closer to the center of mass than the average radius of the cluster ($r_{cluster,avg}$):

$$r_{buried} < r_{cluster,avg} - r_{cov} \; . \tag{0}$$

Three larger clusters, $In_{10}P_{10}$, $In_{13}P_{13}$ and $In_{14}P_{14}$ have buried atoms with one buried P in $In_{10}P_{10}$, and both In and P buried in $In_{13}P_{13}$ and $In_{14}P_{14}$ (see Supporting Information Table S10). Surface atoms in the larger-sized clusters have average CNs ranging from 2.7 to 3.5 for In atoms and 3.0 to 3.3 for P atoms and average In-P nearest neighbor distances of 2.5-2.6 Å, slightly shorter than average In-P bond distance of 2.6-2.8 Å for buried atoms (see Supporting Information Table S11). Overall, while relatively few clusters have a large core of buried atoms, most clusters with more than 18 atoms have a majority of CN=3 or higher atoms, and the few cases with anomalously low energy (e.g. In_9P_9) correspond to a high number such atoms.

3c. Testing the influence of alternative starting configurations

In order to identify how sensitive the final energy and geometric structures of clusters are to the initial configurations, we compare results obtained with four additional initial configurations (see Figure 1 and Supporting Information Figure S6). Two of the structures are generated from single layer surface models of InP, including: i) a 28 atom layer of InP(011) and ii) a 32 atom layer of InP(001), while the third model is a 26 atom spherical cut of bulk InP and the fourth model is a liquid-like structure (see Supporting Information for details). The coordination numbers of the initial structures are highest in the bulk model case ($In_{13}P_{13}$) at two to four for both In and P, intermediate and comparable to InP(111) in the $In_{14}P_{14}$ model (two to three for In and P) and liquid-like structures, and lowest in the $In_{16}P_{16}$ model at one to two for

15

both In and P. The bulk model is the most compact (10.5 Å diameter) while both $In_{14}P_{14}$ and $In_{16}P_{16}$ are flat, rectangular structures. Comparing AIMD simulations, we observe a shorter time to coalescence (3 ps) for the bulk models and liquid-like models than for the InP(111) model, likely owing to shorter initial distances, while for $In_{14}P_{14}$ initial average distances are more comparable to InP(111) and the time to coalescence (5 ps) is similar. For the largest cluster studied here ($In_{16}P_{16}$), a 6 ps coalescence and stabilization run requires around 11 days of computer time on two nVidia GeForce GTX Titan GPUs, motivating the accelerated approaches we introduce later in Section 3d.

Interestingly, energetic and structural properties for the clusters generated from these differing starting structures are quite similar. Final optimized relative energies are within 2 kcal/mol per pair, with the spherical bulk structure slightly lower by 1 kcal/mol per pair with respect to InP(111) and the InP(011) structure and liquid-like structures slightly higher by 1 kcal/mol per pair. These differences are well within the uncertainty of the choice of other simulation parameters. As expected from energetic comparisons, average distances are similar (see Supporting Information Table S12), as are average coordination numbers ($In_{13}P_{13}$: 3.3 for both In and P in spherical bulk, 3.3 for In and 3.5 for P in InP(111); $In_{14}P_{14}$: 3.1 for both In and P in InP(011) and InP(111)). Differences in CN arise from formation of a P-P dimer in the InP(111)-derived $In_{13}P_{13}$ cluster (see Supporting Information Table S12). While the starting configuration for our liquid-like model contains both In-In and P-P coordination, the final structure contains only P-P dimers and no remaining In-In coordination. As a result, the average coordination numbers for In are slightly lower at 2.7 as compared to 2.8-2.9 for other 24 atom clusters, and higher for P at 3.7 compared to the crystalline structures (see Supporting Information Table S12). We emphasize here that despite a short coalescence time for the

16

spherical bulk model, the final structure is in fact amorphous in nature and comparable to those obtained from other starting configurations. Overall, differing initial configurations have a limited effect on the final energy and geometry of clusters, emphasizing the robustness of this scheme for sampling low-energy geometries.

3d. Accelerating cluster structure generation

Thus far, our approach has required 2.5 to 15 ps of AIMD sampling for each cluster size. As an alternative, it may be possible to generate new clusters starting from optimized clusters of a different size. Using the adding approach (Figure 4), we generate larger starting clusters for AIMD by identifying In and P atoms with the lowest coordination number at the surface of the cluster. Surface atoms are identified as those with a distance to the center of mass larger than the average radius of the cluster. In some cases (e.g. In_7P_7), there is only one pair of P and In with the minimum coordination number (here, CN=2), while for others (e.g. In_9P_9), several (here, 3) surface sites have the same coordination (here, CN=3), of which one is randomly selected. The additional In (P) atom is placed along the vector between the P (In) site and the center of mass at a distance of 3 Å from the surface. New initial In_4P_4 to $In_{13}P_{13}$ configurations from InP(111)-derived clusters (Sec. 3b) and $In_{14}P_{14}$ to $In_{17}P_{17}$ from the alternative starting configurations (Sec. 3c) are used as starting points for AIMD runs and subsequent optimizations. The resulting energy of the structures obtained from the adding (also referred to as "single adding", SA) method is within 3.7 kcal/mol per pair of the results obtained directly from crystal model structures, except for the smallest structure, In_4P_4 (see Supporting Information Table S13). Typically, the energies of structures obtained with the adding method are lower than those obtained directly from rearrangement of crystal-derived models.
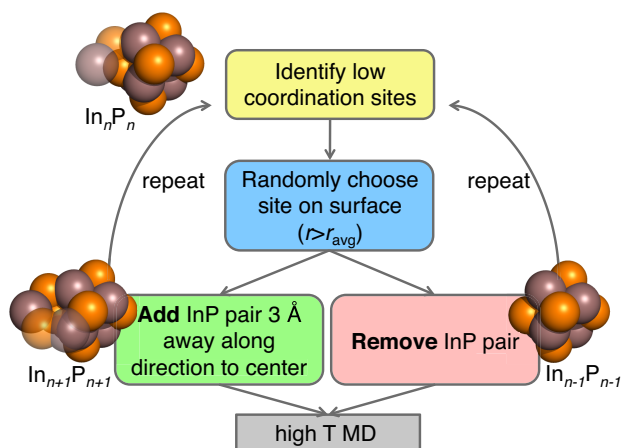
Figure 4. Flowchart schematic for adding and removing pairs of In and P to generate new initial structures for *ab initio* molecular dynamics from clusters at a given size. A representative starting structure (In_nP_n) is shown at top with the atoms removed ($In_{n-1}P_{n-1}$, bottom right) shown with translucent spheres and the added atoms to the larger cluster ($In_{n+1}P_{n+1}$, bottom left) also indicated with translucent spheres. Indium is depicted as an opaque or translucent brown van der Waals sphere, and phosphorus is shown as an opaque or translucent orange van der Waals sphere.

For the generation of larger clusters, we added two atom pairs ("double adding" or DA) to generate In_5P_5 to $In_{16}P_{16}$ and $In_{18}P_{18}$ from smaller clusters and added three to six atom pairs (multiple adding, "MA") to generate $In_{19}P_{19}$ to $In_{22}P_{22}$ clusters. On average, energies per InP pair of the DA structures are slightly higher than those obtained with SA for In_5P_5 to $In_{15}P_{15}$ with an average deviation of 1.1 kcal/mol and maximum difference of 4.3 kcal/mol (for In_7P_7, see Supporting Information Table S14). Energetic differences are a result of differing coordination environment: the SA cluster CN is more uniform with CN=3 for all but one In CN=2 (1;2) and P CN=4 (4;5), while the DA cluster has only two CN=3 In and P atoms and more low-coordinated (CN=2) In (four atoms) or P (three atoms) and high-coordinated (one CN=4 for In, two CN=5 for

18

P) atoms. Interestingly, in both clusters, P-P dimers are observed (1 for SA, 2 for DA). A benefit of the MA approach is the size of clusters we are able to generate low-energy structures for as our 44 atom cluster is 1.5 nm in diameter, on the smaller side of experimental[14] nanoparticles. For the largest clusters, the average In CN is 2.8-3.3 and P CN is 3.1-3.8, within reasonable agreement to experimental coordination number averages of 3.56 for bulk amorphous InP[68].

In addition to having comparable energetics, the SA, DA, and MA AIMD runs exhibit dramatically shorter coalescence times on the order of 0.5 to 1 ps (see Supporting Information Table S15). For these approaches, the predominant rearrangement during AIMD is around the site of the newly added atoms. We quantify movements of each atom as the change in distance to the center of mass of the original cluster during the AIMD trajectory. For instance, in the SA trajectory for $In_{12}P_{12}$, the change in distance for the four adjacent atoms to the newly added atoms is larger than 0.9 Å, while the movements of other atoms are < 0.5 Å. This limited rearrangement is the source of reduced computational effort for all clusters generated in this manner. Shorter coalescence times with the adding method provide a path toward generating large clusters on the order of the 2-4 nm range generated experimentally[14] by adding several pairs of atoms at a time and running brief 1 ps dynamics intervals and geometry optimizations for relaxation after each set of atoms has been added. While computational cost of the underlying electronic structure calculations will increase with increasing system size, brief dynamics runs remain feasible for these larger system sizes. Unlike the adding methods, coalescence times from AIMD of InP(111) models increase significantly with increasing system size. By fitting to symmetric InP(111) model coalescence times (see Supporting Information Table S5), we extrapolate that a 2 nm $In_{52}P_{52}$ cluster will require 88 ps of coalescence time. While GPU-accelerated electronic structure calculations generally only scale $O(N^2)$ with the number of basis functions[53], the

quadratic scaling of coalescence time with the number of atoms will limit AIMD starting from crystalline models to smaller cluster sizes. Therefore, in order to reach a 2-3 nm cluster size comparable to experimentally synthesized clusters, a sequential adding approach with brief periods of dynamics between each adding step starting from a mid-sized cluster (e.g. ~40 atoms) will greatly reduce the computational cost.

Coordination numbers in clusters generated from all adding methods exhibit a wider range for In (both lower and higher CN) but overall comparable average CN to those obtained from longer MD runs. The SA, DA, and MA clusters have higher average CNs for P due to the increased presence of P-P dimers (see Supporting Information Table S16), with almost all clusters having at least one but as many as nine (in $In_{22}P_{22}$). For the larger clusters ($In_{15}P_{15}$-$In_{22}P_{22}$), the average CN is between 2.8 to 3.3 (2.1 to 3.0; 3.0 to 3.4) for In atoms and 3.1 to 3.8 (3.0 to 3.2; 3.1 to 4.0) for P atoms compared to a larger range of 2.0 to 3.5 for the average CN and smaller lower limit on the CN (1.9 to 3.2 for In, 2.0 to 3.5 for P; 2.0 to 3.5 for In, 2.0 to 4.5 for P) for the smaller clusters. The overall number of buried atoms also increases, with the largest model having 5 (4; 5) buried In atoms and 5 (2; 5) buried P atoms (see Supporting Information Table S17).

We also generated new structures by removing pairs of atoms on the optimized clusters (see Figure 4) to test whether this approach accelerates generation of comparable, low-energy clusters. As before, we identify pairs of In and P atoms with the lowest CN and now remove them from the cluster. We used an $In_{13}P_{13}$ cluster to generate In_3P_3 to $In_{12}P_{12}$ and an $In_{16}P_{16}$ cluster to generate In_5P_5 to $In_{15}P_{15}$ starting structures by repeatedly removing atoms. As with the adding method, coalescence times were significantly reduced, with the longest 2.5 ps time, which was for In_5P_5 generated from $In_{16}P_{16}$, likely due to an unfavorable starting configuration from large

numbers of removed atoms (see Supporting Information Table S18). The energies of removing method structures were on average within 1.6 kcal/mol per pair of the other methods and comparable to those obtained from crystal models but slightly higher than those obtained from the adding method. The removing approach may be suitable for generating clusters for which no symmetric initial configuration is available. The most elongated InP(111) model required 15 ps for coalescence, while the two structures generated by the removing method coalesced within 0.5-1.5 ps, and final energies agreed within 1.7 kcal/mol for all three structures. Consistent with energetic observations, the overall CNs for the structures generated with the removing method were comparable to those obtained directly and from the adding approach. Phosphorus dimers, which were present in the starting structures, were preserved in many of the new clusters.

3e. Comparing properties of clusters

Having employed up to five different approaches for a single system size, there are 66 clusters 6-44 atoms in size for which the relative energetics may be directly compared (Figure 5). While it was previously noted that the adding approach yields lower-energy structures, there is no single approach that consistently yields the lowest energy structure. The largest energy variation (8 kcal/mol) is observed for In_4P_4, for which a high-energy structure is characterized by all CN=3 atoms, while the lowest energy structure corresponds to CN=2 for all In and an even mix of CN=3 and CN=4 for P atoms, with the higher CN for P resulting from P-P dimers. The variation in energy per pair from In_5P_5 to $In_{16}P_{16}$ between up to five methods is around 1.3-4.3 kcal/mol. As cluster size increases, the variation in energy of the clusters obtained with the different approaches decreases, and variations narrow considerably for cluster sizes 20 atoms or above. One exception is In_9P_9 with an energy range of 5.0 kcal/mol across methods, which is larger than the 1.3-2.0 kcal/mol variation for comparably sized clusters (e.g. In_8P_8, $In_{12}P_{12}$,

21

$In_{13}P_{13}$). For the 18 atom cluster, higher energy structures have CN=1 and CN=2 In atoms absent from the lowest energy structure.
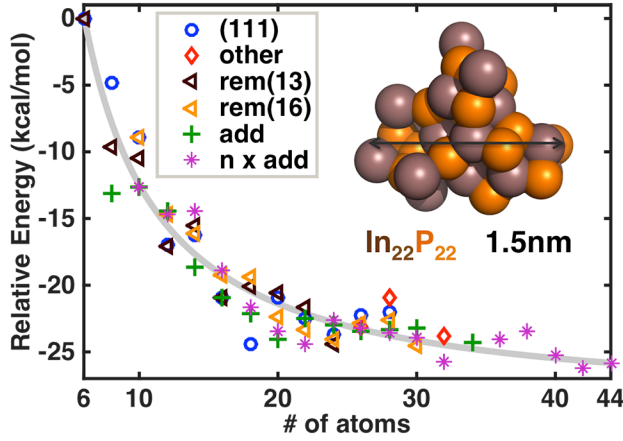
Figure 5. Relative energy per pair of InP atoms (referenced against the In_3P_3 cluster) for geometry optimized clusters obtained from *ab initio* molecular dynamics sampling for clusters from 6 atoms to 44 atoms in size. Results are categorized based on the approach for generating the initial structure: from a layer of InP(111) (blue circles); $In_{13}P_{13}$ from a spherical cut of bulk (red diamonds), $In_{14}P_{14}$ from a layer of InP(011) (red diamonds), or $In_{16}P_{16}$ from a layer of InP(001) (red diamonds); using the removing method starting from the $In_{13}P_{13}$ cluster (brown triangles); using the removing method starting from the $In_{16}P_{16}$ cluster (yellow triangles), using the adding method to generate a structure with $n+1$ pairs from a structure with n pairs (green crosses), and using multiple adding methods with various initial structures (pink stars). A best-fit exponential curve is shown in gray. The resulting structure of one representative cluster ($In_{22}P_{22}$, In atoms in brown and P atoms are shown in orange) and its size is provided in the inset.

The size-dependence of relative energies from data on all clusters has a best fit exponentially decaying trend line of the form:

$$E_{per\,pair}(n) = 218(2n)^{-1.12} - 29 \quad , \tag{0}$$

22

where the asymptotic relative energy per pair is -29 kcal/mol and clusters $In_{61}P_{61}$ or larger are predicted to be within 1 kcal/mol of the asymptote. This trend line is comparable to the one obtained from 6-28 atom InP(111) models, suggesting that cluster properties are converging by around 28 atoms, although this enlarged fit has slightly steeper dependence on size and a shallower asymptote. The computed energy per pair is relatively flat for all clusters larger than 8 pairs of InP atoms, consistent with the trend line equation that shows the relative energy changes by less than 1 kcal/mol per pair for clusters 18 atoms or larger. Such observations are consistent with previous tight binding calculations by Roy and Springborg[28] that also showed similar energetic decreases with increasing system size, though we note in that case geometry optimizations were carried out rather than full AIMD-based rearrangements.

The In-P, In-In, and P-P radial distribution functions (RDF) for all generated clusters (Figure 6; In-P bin size 0.13 Å, In-In and P-P bin size 0.24 Å) reveal overall structural characteristics. The In-P RDF is peaked at 2.5 Å, in agreement with experimental[42] 2.5 Å nearest neighbor distances in the bulk structure, and the RDF first minimum is around 3.1 Å, supporting the distance cutoff choice for coordination number. A broad second shell feature from 4.5 Å to 7 Å is centered around 5.7 Å, which is a larger distance than the experimental[42] second-sphere distance peak at 4.8 Å. The P-P RDF exhibits a small peak at around 2.1 Å, due to the 116 P-P dimers observed in the clusters. The same behavior is not present in the In-In RDF, where no indium dimers are observed. The same-species RDFs have first non-bonded peaks at 3.6 Å (In-In) and 4.5 Å (P-P), and second peaks centered at 5.8 Å (In-In) and 7.1 Å (P-P). Overall, the P-P RDF peaks are at larger distances than In-In, consistent with earlier observations of differences in average distances in the MD simulations (see Figure 2) and in agreement with observations of previous tight-binding geometry optimizations[28]. These larger P-P distances do not necessarily

mean that phosphorus atoms aggregate on the surface. In and P atoms have comparable probabilities in the distance to the cluster center of mass (see Supporting Information Figure S7) for short and very long distances. While intermediate layers may be segregated with more of one element or the other, core and surface atom numbers are comparable for In and P.
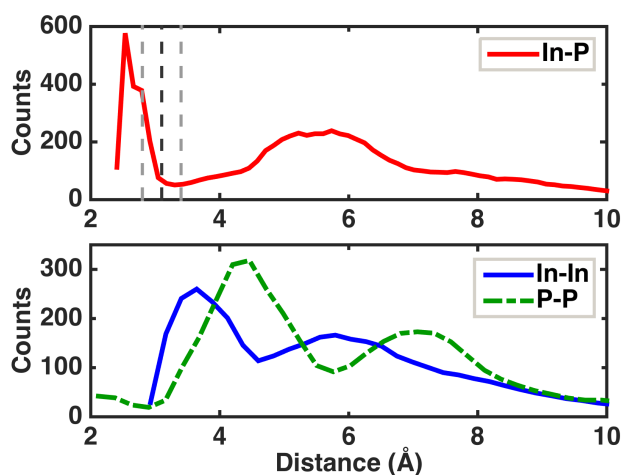
Figure 6. The radial distribution functions for (top) In-P distances (red solid line), and (bottom) In-In (blue solid line) or P-P (green dashed line) distances compared over all geometry optimized InP clusters (size range = 6-44 atoms) from all *ab initio* molecular dynamics sampling runs. The nearest neighbor cutoff we define for In-P distances is indicated at top by a black dashed line alongside upper and lower bounds for nearest neighbor cutoffs (gray dashed lines).

In order to identify whether features of RDFs are size-dependent, we group clusters as "small" (3-7 pairs), "intermediate" (8-14), and "large" (15-22), based in part on energetic trends (Figure 5). A comparison of RDFs for these three groups (see Supporting Information Figure S8) reveals that small clusters have a shorter distance for the first-minimum in the In-P RDF, which is below 3.1 Å. The first minimum in the In-P RDF then increases for intermediate clusters and is larger than 3.1 Å for the largest clusters. For In-In and P-P RDFs, the only difference is

increasingly large second non-bonding peaks, which must occur as cluster size increases. Therefore, energetic differences in clusters are driven more by uncoordinated surface sites than by geometric differences in nearest neighbor interactions.

Evaluation of overall cluster structural properties reveals high coordination number (CN) around select In and P atoms. Indium CNs range from 1 to 5, with three cases of CN=5 atoms observed in the clusters. The phosphorus atom CNs have a larger range from 2 to 7, with 3 CN=7 P atoms and 6 CN=6 P atoms. We designate short In-P bond distances as $d \leq 2.75$ Å and long In-P bonds as those with $d > 2.75$ Å. A representative CN=7 P (Figure 7) is characterized by two short In-P bonds with $d_{avg} = 2.69$ Å and five long In-P bonds with d_{avg}=2.92 Å, while CN=6 P (Figure 7) has three short In-P bonds ($d_{avg} = 2.67$ Å) and three longer In-P bonds ($d_{avg} = 2.90$ Å). For CN=5 P, In-P bonds are even shorter with four short d_{avg}= 2.59 Å bonds and one longer 2.77 Å bond, consistent with the presence of long bonds appearing primarily in high CN cases. For a representative CN=5 In, bond distances are similar to the CN=5 P case but with three shorter In-P bonds (d_{av}=2.63 Å) and two longer In-P bonds (d_{av}=2.82 Å). In the crystal structure, In and P are each four-coordinated in a tetrahedral configuration. Our clusters contain a large number of four-coordinated species in two distinct geometries, neither of which perfectly replicate the tetrahedral crystal environment coordination. In the first case, In and P atoms have a quasi-tetrahedral shape (see Figure 7) with three short bonds (d_{av}=2.60 Å for In and d_{av}=2.64 Å for P) and one long bond (d=3.00 Å for In and d=2.85 Å for P). In the other CN=4 case, the coordinating atoms are all to one side of the likely surface atom, described either by all short bonds (d_{av}=2.64 Å for P) or three short (d_{av}=2.61 Å for In) and one long bond (d=3.02 Å for In).
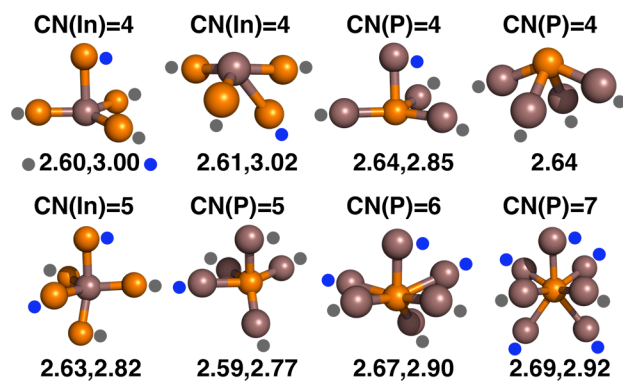
Figure 7. Representative configurations of In and P atoms with coordination number (CN) equal to or larger than 4: two In atoms with CN=4 (top left), two P atoms with CN=4 (top right), one In atom with CN=5 (bottom left), one P atom with CN=5 (bottom left), one P atom with CN=6 (bottom right), one P atom with CN=7 (bottom right). Indium atoms are brown and phosphorus atoms are indicated in orange. Short In-P bond distances (r<2.75 Å) are indicated by gray dots and long In-P bond distances (r>2.75 Å) are indicated by blue dots. Separate averages of the short and long bond distances are shown underneath for each configuration.

In order to further characterize structural properties of these amorphous nanostructures, we have carried out Voronoi polyhedron analysis[64, 69]. The polyhedron surrounding each atom is formed by its nearest neighbors and can therefore provide additional insight into the coordination environment. As the cluster size increases, the maximum number of edges on each face for In atoms and P atoms increases from 7 and 6, respectively, to about 10 indicating high-coordinated atoms (see Supporting Information Figure S9). Across a wide range of sizes, we observe nearly monotonically increasing average numbers of edges for both In and P atoms, indicating there are more core atoms in large-sized clusters (see Supporting Information Figure S9). These properties level off slightly faster in indium than they do for phosphorus, but the average number of edges for In is slightly larger than P, consistent with previous observation of P-P RDF peaks occurring

26

at larger distances compared to In-In.

Partial charges from NBO analysis demonstrate how coordination environment influences electronic structure (Figure 8). As In coordination number increases, the net charge increases from as low as around +0.75 e- to around +1.25 e-. While there is a variation in charge for different atoms, with the exception of CN=2 In, the distributions are narrow and peaked around one value. At around CN=2, there is a transition between the low-net charge In and high net-charge In, with some CN=2 In charges between these two limits, but for CN>2, the charges are primarily independent of coordination number. Phosphorus charge distributions are complicated by the presence of P-P dimers. For instance, CN=4 P has three peaks: i) at -1.4 e-, corresponding to coordination only by In, ii) at -1.0 e- for 3 In: 1 P coordination, and iii) at -0.5 e- for 2 In : 2 P coordinating the central P atom. The reduced net charge in the presence of additional coordinating phosphorus is also apparent for CN=5 and CN=7 (-1.7-1.8 e- vs. -1.1-1.2 e- with P present). Overall, as CN increases, there is also an increase in average net negative charge for both the pure In-coordinated peak and the partially P-coordinated middle peaks.
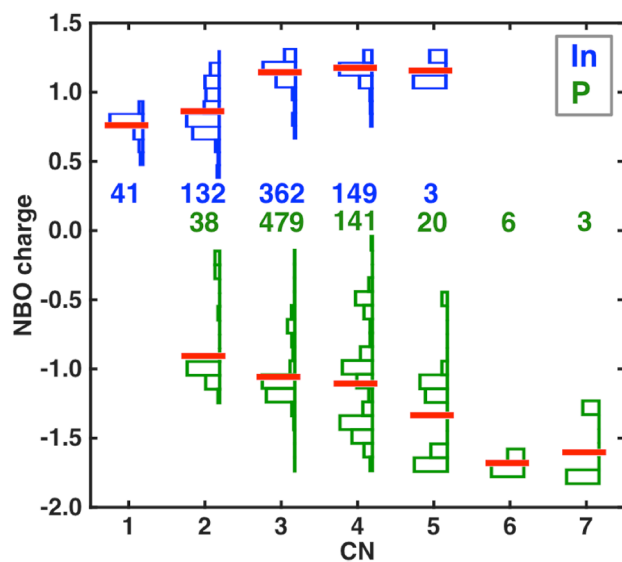
Figure 8. The distribution of partial charges for In atoms (blue, top), and P atoms (green, bottom) grouped by coordination number (In: CN from 1 to 5; P: CN from 2 to 7) and averages of each charge distribution (red lines) compared over all atoms from all optimized InP clusters considered. The charge distributions are adjusted so that peaks are at the same height for all distributions, and counts of each coordination number are shown (beneath distributions for In, above distributions for P).

Until now, we have compared energetic trends only amongst the generated amorphous clusters, but a critical question is whether these structures are lower or higher in energy than ordered, crystalline models of the same size. Symmetric models of bulk InP in the studied size range are 14, 24, 26, and 44 atoms, which range from 7.6 Å to 13.3 Å in diameter before geometry optimization, and the largest two have been previously studied[30]. For consistency, we do not passivate the surfaces of the ordered clusters, but we do geometry optimize the structures and compare to the amorphous structures (Figure 9). Relative energies are evaluated following eqn. 4, and, as a result, the smallest 14 atom unoptimized bulk model has a positive relative energy per pair. The unoptimized structures decrease in energy monotonically to a negative value for the largest 44 atom cluster, though these unoptimized structures have relative energies far above the amorphous clusters. After geometry optimization, energies of the ordered models are lowered on average by -15 kcal/mol per pair, with the energy reduction decreasing as the number of bulk atoms increase in the larger clusters. This energy reduction is associated with rearrangement of atoms that are CN=2 in the initial model to higher-coordinated geometries. Interestingly, the range of relative energies for the amorphous clusters generated previously is consistently below the optimized bulk structures by around 2 to 5 kcal/mol per pair. These

energetic observations confirm that we have generated low energy nanostructures of In and P that exhibit coordination environments different from crystalline InP. Such structures may be favored in high-temperature synthesis or with weak ligands that do not direct and slow InP cluster growth. Colloidal quantum dot synthesis is typically directed by strong ligand interactions absent in our simulations, giving rise to an amorphous surface structure and crystalline core. However, structural motifs we have identified are likely candidates for defects and surface structures even in crystalline QDs due to the favorable energetics we have observed. Alternative experimental techniques such as gas phase condensation from laser evaporated materials[70] and more recently microfluidic nebulator technology[71] have both enabled the direct synthesis of amorphous nanoparticle structures. Overall, these observations suggest that this approach for generating amorphous nanostructures might also be applied to study transition-metal phosphide materials that are experimentally already known to have amorphous character[35].
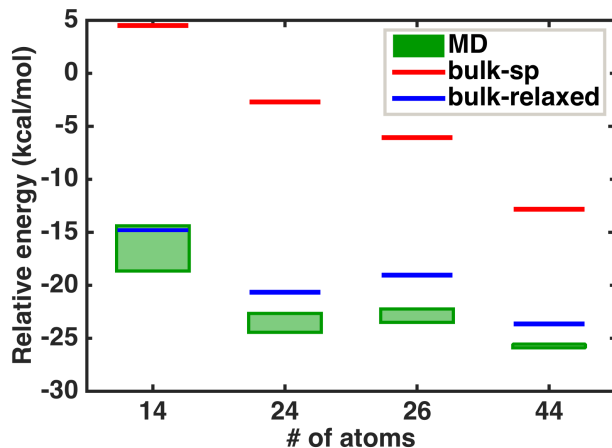
Figure 9. Comparisons of relative energy per pair of InP atoms for clusters from *ab initio* molecular dynamics simulations followed by geometry optimizations (green shaded box indicates an energy range from different approaches) with single point energy (red lines) and geometry optimized (blue lines) clusters obtained from spherical cuts of InP bulk (In_7P_7, $In_{12}P_{12}$, $In_{13}P_{13}$, and $In_{22}P_{22}$). The zero relative energy per pair reference is taken as the energy of the

In$_3$P$_3$ optimized cluster, as discussed in the text.

4. Conclusions

We have introduced a high-temperature *ab initio* molecular dynamics approach for the sampling and discovery of low-energy indium phosphide nanostructures. Starting from open, flat single layer models of crystalline InP, we observed consistent rearrangement to globular, amorphous clusters over a wide size range (8-44 atoms), with exceptions in this trend occurring only for the smallest models considered (6 or 10 atoms). We tracked this rearrangement through observation of a linear decline in average distances in the rearranging cluster that we referred to as coalescence followed by a stabilized regime in which distances fluctuated around constant averages. The time for coalescence depended primarily on the shape of the initial structure and secondarily on system size. When comparing outcomes from differing initial structures, we observed a narrow range in relative energies between clusters. We further identified computational cost reductions in our approach by adding or removing atoms from converged clusters and re-initiating the AIMD step, dramatically reducing the time to coalescence without strongly affecting the final geometric or electronic structure. Accelerated, sequential adding of pairs to grow clusters is likely necessary to study larger clusters in the 2-4 nm range that is more comparable with experimentally synthesized clusters. We note that while coalescence time of direct AIMD simulations from crystalline models grows substantially with system size, sequential adding dynamics relaxation times remain around 1 ps regardless of system size. By harnessing efficiently scaling electronic structure approaches, this efficient rearrangement will enable study of large clusters up to a few hundred atoms as well as efficient screening of properties of a wider array of compounds.

Relative energetics of these structures were strongly size-dependent up to around 20 atoms as average coordination numbers increased dramatically from CN=2 to around CN=3-4. Unusual coordination environments that lowered energy in the clusters included the formation of phosphorus-phosphorus dimers and high-coordination numbers: up to five-coordinated indium and six- or seven-coordinated phosphorus, with alternating short and long bond distances to describe the coordination environment. Although a fair number of four-coordinated In and P were present in the amorphous clusters, few, if any resembled the tetrahedral coordination present in the InP crystal. Despite the unusual coordination present in these structures, a comparison to bulk models both at experimental geometries and after optimization indicated that the sampled, amorphous structures are consistently lower in energy. Moving forward, our approach is promising for the sampling of low-energy models of amorphous nanostructures, such as those observed in transition-metal phosphides and borides[35].

ASSOCIATED CONTENT

Supporting Information. Initial configurations and selected final structures of InP(111) models; simulation timing (coalescence time, stabilization time) in AIMD for different models; geometry parameters (CN, diameter, buried/surface atoms), NBO charge and energetics compared over different models and initial configurations; energies at different simulation temperature; distances of In and P atoms to cluster center of mass; radial distribution functions of different cluster size groupings. This material is available free of charge via the Internet at http://pubs.acs.org.

AUTHOR INFORMATION

Corresponding Author

*email:hjkulik@mit.edu, phone: 617-253-4584

Notes

The authors declare no competing financial interest.

ACKNOWLEDGMENT

REFERENCES

1.   Talapin, D. V.; Lee, J.-S.; Kovalenko, M. V.; Shevchenko, E. V., Prospects of Colloidal Nanocrystals for Electronic and Optoelectronic Applications. *Chemical reviews* **2009**, *110*, 389-458.
2.   Michalet, X.; Pinaud, F. F.; Bentolila, L. A.; Tsay, J. M.; Doose, S.; Li, J. J.; Sundaresan, G.; Wu, A. M.; Gambhir, S. S.; Weiss, S., Quantum Dots for Live Cells, in Vivo Imaging, and Diagnostics. *science* **2005**, *307*, 538-544.
3.   Parak, W. J.; Gerion, D.; Pellegrino, T.; Zanchet, D.; Micheel, C.; Williams, S. C.; Boudreau, R.; Le Gros, M. A.; Larabell, C. A.; Alivisatos, A. P., Biological Applications of Colloidal Nanocrystals. *Nanotechnology* **2003**, *14*, R15.
4.   Sun, Q.; Wang, Y. A.; Li, L. S.; Wang, D.; Zhu, T.; Xu, J.; Yang, C.; Li, Y., Bright, Multicoloured Light-Emitting Diodes Based on Quantum Dots. *Nature Photonics* **2007**, *1*, 717-722.
5.   Caruge, J.; Halpert, J.; Wood, V.; Bulović, V.; Bawendi, M., Colloidal Quantum-Dot Light-Emitting Diodes with Metal-Oxide Charge Transport Layers. *Nature Photonics* **2008**, *2*, 247-250.
6.   Semonin, O. E.; Luther, J. M.; Choi, S.; Chen, H.-Y.; Gao, J.; Nozik, A. J.; Beard, M. C., Peak External Photocurrent Quantum Efficiency Exceeding 100% Via Meg in a Quantum Dot Solar Cell. *Science* **2011**, *334*, 1530-1533.
7.   Kamat, P. V., Quantum Dot Solar Cells. Semiconductor Nanocrystals as Light Harvesters†. *The Journal of Physical Chemistry C* **2008**, *112*, 18737-18753.
8.   Klimov, V.; Mikhailovsky, A.; Xu, S.; Malko, A.; Hollingsworth, J.; Leatherdale, C.; Eisler, H.-J.; Bawendi, M., Optical Gain and Stimulated Emission in Nanocrystal Quantum Dots. *Science* **2000**, *290*, 314-317.
9.   Nanda, J.; Ivanov, S. A.; Achermann, M.; Bezel, I.; Piryatinski, A.; Klimov, V. I., Light Amplification in the Single-Exciton Regime Using Exciton-Exciton Repulsion in Type-Ii Nanocrystal Quantum Dots. *The Journal of Physical Chemistry C* **2007**, *111*, 15382-15390.

10.	Murray, C. B.; Norris, D. J.; Bawendi, M. G., Synthesis and Characterization of Nearly Monodisperse Cde (E = Sulfur, Selenium, Tellurium) Semiconductor Nanocrystallites. *Journal of the American Chemical Society* **1993**, *115*, 8706-8715.

11.	Dabbousi, B.; Rodriguez-Viejo, J.; Mikulec, F. V.; Heine, J.; Mattoussi, H.; Ober, R.; Jensen, K.; Bawendi, M., (Cdse) Zns Core-Shell Quantum Dots: Synthesis and Characterization of a Size Series of Highly Luminescent Nanocrystallites. *The Journal of Physical Chemistry B* **1997**, *101*, 9463-9475.

12.	Kirchner, C.; Liedl, T.; Kudera, S.; Pellegrino, T.; Muñoz Javier, A.; Gaub, H. E.; Stölzle, S.; Fertig, N.; Parak, W. J., Cytotoxicity of Colloidal Cdse and Cdse/Zns Nanoparticles. *Nano letters* **2005**, *5*, 331-338.

13.	Yang, X.; Zhao, D.; Leck, K. S.; Tan, S. T.; Tang, Y. X.; Zhao, J.; Demir, H. V.; Sun, X. W., Full Visible Range Covering Inp/Zns Nanocrystals with High Photometric Performance and Their Application to White Quantum Dot Light-Emitting Diodes. *Advanced Materials* **2012**, *24*, 4180-4185.

14.	Cros-Gagneux, A.; Delpech, F.; Nayral, C.; Cornejo, A.; Coppel, Y.; Chaudret, B., Surface Chemistry of Inp Quantum Dots: A Comprehensive Study. *Journal of the American Chemical Society* **2010**, *132*, 18147-18157.

15.	Adam, S.; Talapin, D.; Borchert, H.; Lobo, A.; McGinley, C.; de Castro, A.; Haase, M.; Weller, H.; Möller, T., The Effect of Nanocrystal Surface Structure on the Luminescence Properties: Photoemission Study of Hf-Etched Inp Nanocrystals. *The Journal of chemical physics* **2005**, *123*, 084706.

16.	Allen, P. M.; Walker, B. J.; Bawendi, M. G., Mechanistic Insights into the Formation of Inp Quantum Dots. *Angewandte Chemie International Edition* **2010**, *49*, 760-762.

17.	Gary, D. C.; Terban, M. W.; Billinge, S. J.; Cossairt, B. M., Two-Step Nucleation and Growth of Inp Quantum Dots Via Magic-Sized Cluster Intermediates. *Chemistry of Materials* **2015**, *27*, 1432-1441.

18.	Xie, R.; Li, Z.; Peng, X., Nucleation Kinetics Vs Chemical Kinetics in the Initial Formation of Semiconductor Nanocrystals. *Journal of the American Chemical Society* **2009**, *131*, 15457-15466.

19.	Karanth, D.; Fu, H., Polarization Ratio and Effective Mass in Inp Nanowires: Effect of Crystallographic Axis. *Physical Review B* **2006**, *74*, 155312.

20.	Schmidt, T., Hydrogen and Oxygen on Inp Nanowire Surfaces. *Applied physics letters* **2006**, *89*, 123117.

21.	Li, D.; Wang, Z.; Gao, F., First-Principles Study of the Electronic Properties of Wurtzite, Zinc-Blende, and Twinned Inp Nanowires. *Nanotechnology* **2010**, *21*, 505709.

22.	Chandiramouli, R., Band Structure and Transport Studies on Inp Nanotube–a First-Principles Investigation. *Superlattices and Microstructures* **2015**, *83*, 193-209.

23.	Dos Santos, C. L.; Piquini, P., Diameter Dependence of Mechanical, Electronic, and Structural Properties of Inas and Inp Nanowires: A First-Principles Study. *Physical Review B* **2010**, *81*, 075408.

24.	Shu, H.; Chen, X.; Zhou, X.; Lu, W., Spatial Confinement of Carriers and Tunable Band Structures in Inas/Inp-Core–Shell Nanowires. *Chemical Physics Letters* **2010**, *495*, 261-265.

25.	Wood, B. C.; Ogitsu, T.; Schwegler, E., Local Structural Models of Complex Oxygen- and Hydroxyl-Rich Gap/Inp (001) Surfaces. *The Journal of chemical physics* **2012**, *136*, 064705.

26. Wood, B. C.; Schwegler, E.; Choi, W. I.; Ogitsu, T., Hydrogen-Bond Dynamics of Water at the Interface with Inp/Gap (001) and the Implications for Photoelectrochemistry. *Journal of the American Chemical Society* **2013**, *135*, 15774-15783.

27. Wood, B. C.; Schwegler, E.; Choi, W. I.; Ogitsu, T., Surface Chemistry of Gap (001) and Inp (001) in Contact with Water. *The Journal of Physical Chemistry C* **2014**, *118*, 1062-1070.

28. Roy, S.; Springborg, M., Theoretical Study of Structural and Electronic Properties of Naked Stoichiometric and Nonstoichiometric Indium Phosphide Clusters. *The Journal of Physical Chemistry B* **2003**, *107*, 2771-2779.

29. Roy, S.; Springborg, M., Theoretical Investigation of the Influence of Ligands on Structural and Electronic Properties of Indium Phosphide Clusters. *The Journal of Physical Chemistry A* **2005**, *109*, 1324-1329.

30. Cho, E.; Jang, H.; Lee, J.; Jang, E., Modeling on the Size Dependent Properties of Inp Quantum Dots: A Hybrid Functional Study. *Nanotechnology* **2013**, *24*, 215201.

31. Abuelela, A. M.; Mohamed, T. A.; Prezhdo, O. V., Dft Simulation and Vibrational Analysis of the Ir and Raman Spectra of a Cdse Quantum Dot Capped by Methylamine and Trimethylphosphine Oxide Ligands. *The Journal of Physical Chemistry C* **2012**, *116*, 14674-14681.

32. Isborn, C. M.; Kilina, S. V.; Li, X.; Prezhdo, O. V., Generation of Multiple Excitons in Pbse and Cdse Quantum Dots by Direct Photoexcitation: First-Principles Calculations on Small Pbse and Cdse Clusters. *The Journal of Physical Chemistry C* **2008**, *112*, 18291-18294.

33. Kilina, S. V.; Kilin, D. S.; Prezhdo, O. V., Breaking the Phonon Bottleneck in Pbse and Cdse Quantum Dots: Time-Domain Density Functional Theory of Charge Carrier Relaxation. *Acs Nano* **2008**, *3*, 93-99.

34. Kim, D.; Kim, D.-H.; Lee, J.-H.; Grossman, J. C., Impact of Stoichiometry on the Electronic Structure of Pbs Quantum Dots. *Physical review letters* **2013**, *110*, 196802.

35. Carenco, S.; Portehault, D.; Boissière, C.; Mézailles, N.; Sanchez, C., Nanoscaled Metal Borides and Phosphides: Recent Developments and Perspectives. *Chemical Reviews* **2013**, *113*, 7981-8065.

36. Woodley, S. M.; Catlow, R., Crystal Structure Prediction from First Principles. *Nature materials* **2008**, *7*, 937-946.

37. Zhai, H.; Ha, M.-A.; Alexandrova, A. N., Affck: Adaptive Force Field-Assisted Ab Initio Coalescence Kick Method for Global Minimum Search. *Journal of Chemical Theory and Computation* **2015**.

38. Shen, D.; Kong, C.; Jia, R.; Fu, P.; Zhang, H.-X., Investigate the Properties of Mgn Clusters and Their Hydrogen-Storage Mechanism: A Study Based on Dft and a Global Minimum Optimization Method. *The Journal of Physical Chemistry A* **2015**.

39. Muz, İ.; Canko, O.; Atiş, M.; Kamil Yıldırım, E., Search for the Global Minimum Structures of Alb3h2n (N= 0– 6) Clusters. *Journal of computational chemistry* **2014**.

40. Tai, T. B.; Nguyen, M. T., A Stochastic Search for the Structures of Small Germanium Clusters and Their Anions: Enhanced Stability by Spherical Aromaticity of the Ge10 and Ge122− Systems. *Journal of Chemical Theory and Computation* **2011**, *7*, 1119-1130.

41. Assadollahzadeh, B.; Schwerdtfeger, P., A Systematic Search for Minimum Structures of Small Gold Clusters Aun (N= 2–20) and Their Electronic Properties. *The Journal of chemical physics* **2009**, *131*, 064306.

42.   Rapallo, A.; Rossi, G.; Ferrando, R.; Fortunelli, A.; Curley, B. C.; Lloyd, L. D.; Tarbuck, G. M.; Johnston, R. L., Global Optimization of Bimetallic Cluster Structures. I. Size-Mismatched Ag–Cu, Ag–Ni, and Au–Cu Systems. *The Journal of chemical physics* **2005**, *122*, 194308.

43.   Johnston, R. L., Evolving Better Nanoparticles: Genetic Algorithms for Optimising Cluster Geometries. *Dalton Transactions* **2003**, 4193-4207.

44.   Goedecker, S.; Hellmann, W.; Lenosky, T., Global Minimum Determination of the Born-Oppenheimer Surface within Density Functional Theory. *Physical review letters* **2005**, *95*, 055501.

45.   Pietrucci, F.; Andreoni, W., Graph Theory Meets Ab Initio Molecular Dynamics: Atomic Structures and Transformations at the Nanoscale. *Physical review letters* **2011**, *107*, 085504.

46.   Kim, H. G.; Choi, S. K.; Lee, H. M., New Algorithm in the Basin Hopping Monte Carlo to Find the Global Minimum Structure of Unary and Binary Metallic Nanoclusters. *The Journal of chemical physics* **2008**, *128*, 144702-144702.

47.   Borbón-González, D. J.; Fortunelli, A.; Barcaro, G.; Sementa, L.; Johnston, R. L.; Posada-Amarillas, A., Global Minimum Pt13m20 (M= Ag, Au, Cu, Pd) Dodecahedral Core–Shell Clusters. *The Journal of Physical Chemistry A* **2013**, *117*, 14261-14266.

48.   Andreeva, N. A.; Chaban, V. V., Global Minimum Search Via Annealing. Nanoscale Gold Clusters. *Chemical Physics Letters* **2015**.

49.   Hamad, S.; Catlow, C. R. A.; Spano, E.; Matxain, J. M.; Ugalde, J. M., Structure and Properties of Zns Nanoclusters. *The Journal of Physical Chemistry B* **2005**, *109*, 2703-2709.

50.   Chuvilin, A.; Kaiser, U.; Bichoutskaia, E.; Besley, N. A.; Khlobystov, A. N., Direct Transformation of Graphene to Fullerene. *Nature chemistry* **2010**, *2*, 450-453.

51.   Kästner, J.; Carr, J. M.; Keal, T. W.; Thiel, W.; Wander, A.; Sherwood, P., Dl-Find: An Open-Source Geometry Optimizer for Atomistic Simulations†. *The Journal of Physical Chemistry A* **2009**, *113*, 11856-11865.

52.   Petachem. http://www.petachem.com (accessed Jul. 27, 2015).

53.   Ufimtsev, I. S.; Martinez, T. J., Quantum Chemistry on Graphical Processing Units. 3. Analytical Energy Gradients, Geometry Optimization, and First Principles Molecular Dynamics. *Journal of Chemical Theory and Computation* **2009**, *5*, 2619-2628.

54.   Binkley, J. S.; Pople, J. A.; Hehre, W. J., Self-Consistent Molecular-Orbital Methods .21. Small Split-Valence Basis-Sets for 1st-Row Elements. *Journal of the American Chemical Society* **1980**, *102*, 939-947.

55.   Stephens, P. J.; Devlin, F. J.; Chabalowski, C. F.; Frisch, M. J., Ab Initio Calculation of Vibrational Absorption and Circular Dichroism Spectra Using Density Functional Force Fields. *The Journal of Physical Chemistry* **1994**, *98*, 11623-11627.

56.   Lee, C.; Yang, W.; Parr, R. G., Development of the Colle-Salvetti Correlation-Energy Formula into a Functional of the Electron Density. *Physical Review B* **1988**, *37*, 785-789.

57.   Becke, A. D., Density-Functional Thermochemistry. Iii. The Role of Exact Exchange. *The Journal of Chemical Physics* **1993**, *98*, 5648-5652.

58.   Vosko, S. H.; Wilk, L.; Nusair, M., Accurate Spin-Dependent Electron Liquid Correlation Energies for Local Spin Density Calculations: A Critical Analysis. *Canadian Journal of Physics* **1980**, *58*, 1200-1211.

59.   Indium Phosphide (Inp) Lattice Parameters, Thermal Expansion. In *Group Iv Elements, Iv-Iv and Iii-V Compounds. Part a - Lattice Properties*, Madelung, O.; Rössler, U.; Schulz, M., Eds. Springer Berlin Heidelberg: 2001; Vol. 41A1a, pp 1-9.

60. Gražulis, S.; Daškevič, A.; Merkys, A.; Chateigner, D.; Lutterotti, L.; Quirós, M.; Serebryanaya, N. R.; Moeck, P.; Downs, R. T.; Le Bail, A., Crystallography Open Database (Cod): An Open-Access Collection of Crystal Structures and Platform for World-Wide Collaboration. *Nucleic acids research* **2012**, *40*, D420-D427.

61. Hanwell, M. D.; Curtis, D. E.; Lonie, D. C.; Vandermeersch, T.; Zurek, E.; Hutchison, G. R., Avogadro: An Advanced Semantic Chemical Editor, Visualization, and Analysis Platform. *J. Cheminformatics* **2012**, *4*, 17.

62. Pyykkö, P.; Atsumi, M., Molecular Single-Bond Covalent Radii for Elements 1–118. *Chemistry – A European Journal* **2009**, *15*, 186-197.

63. The Crystallography Open Database, Cid: 1010146. http://cod.ibt.lt/cod/1010146.html (accessed Jul. 27, 2015).

64. Rycroft, C. H., Voro++: A Three-Dimensional Voronoi Cell Library in C++. *Chaos* **2009**, *19*, 041111.

65. NBO6.0., E. D. Glendening, J, K. Badenhoop, A. E. Reed, J. E. Carpenter, J. A. Bohmann, C. M. Morales, C. R. Landis, and F. Weinhold, Theoretical Chemistry Institute, University of Wisconsin, Madison. 2013.

66. *The Merck Index - an Encyclopedia of Chemicals, Drugs, and Biologicals*.; The Royal Society of Chemistry, 2013.

67. Harmony, M. D.; Laurie, V. W.; Kuczkowski, R. L.; Schwendeman, R.; Ramsay, D.; Lovas, F. J.; Lafferty, W. J.; Maki, A. G., Molecular Structures of Gas-Phase Polyatomic Molecules Determined by Spectroscopic Methods. *Journal of Physical and Chemical Reference Data* **1979**, *8*, 619-722.

68. Glover, C. J.; Ridgway, M. C.; Yu, K. M.; Foran, G. J.; Lee, T. W.; Moon, Y.; Yoon, E., Structural Characterization of Amorphized Inp: Evidence for Chemical Disorder. *Applied Physics Letters* **1999**, *74*, 1713-1715.

69. Finney, J. In *Random Packings and the Structure of Simple Liquids. I. The Geometry of Random Close Packing*, Proceedings of the Royal Society of London A: Mathematical, Physical and Engineering Sciences, The Royal Society: 1970; pp 479-493.

70. Tavakoli, A. H.; Maram, P. S.; Widgeon, S. J.; Rufner, J.; van Benthem, K.; Ushakov, S.; Sen, S.; Navrotsky, A., Amorphous Alumina Nanoparticles: Structure, Surface Energy, and Thermodynamic Phase Stability. *The Journal of Physical Chemistry C* **2013**, *117*, 17123-17130.

71. Amstad, E.; Gopinadhan, M.; Holtze, C.; Osuji, C. O.; Brenner, M. P.; Spaepen, F.; Weitz, D. A., Production of Amorphous Nanoparticles by Supersonic Spray-Drying with a Microfluidic Nebulator. *Science* **2015**, *349*, 956-960.

TOC GRAPHIC